

Lensless Wiener-Khinchin telescope based on high-order spatial autocorrelation of thermal light

ZHENTAO LIU, XIA SHEN, HONGLIN LIU, HONG YU, AND SHENSHENG HAN*

Shanghai Institute of Optics & Fine Mechanics, Chinese Academy of Sciences, Shanghai 201800, China

*Corresponding author: sshan@mail.shcnc.ac.cn

Compiled September 23, 2019

In the development of high resolution optical imaging with lenses, the manufacture of lenses with ultra large aperture, especially for X-ray, turns to be a big challenge. Based on high-order spatial autocorrelation of thermal light, we propose a lensless Wiener-Khinchin telescope, which can acquire an image of an object in a single-shot detection simply with a spatial random phase modulator. Following the principle of classical coherence theory, a theoretical model of lensless Wiener-Khinchin telescope is built and experimentally verified. It provides a theoretical framework for such imaging systems based on wavefront random phase modulation, where a point-to-point correspondence between an object and image planes doesn't exist in first-order field correlation but can be recovered in high-order correlation of light fields. As an incoherent imaging approach illuminated by thermal light, lensless Wiener-Khinchin telescope can be applied in many fields like astronomical observations and X-ray imaging. © 2019 Optical Society of America under the terms of the [OSA Open Access Publishing Agreement](#)

OCIS codes: (110.0110) Imaging systems; (110.1758) Computational imaging; (110.6150) Speckle imaging; (350.1260) Astronomical optics; (290.5825) Scattering theory.

<http://dx.doi.org/10.1364/optica.XX.XXXXXX>

1. INTRODUCTION

Imaging resolution is always an important issue in various fields of scientific researches and engineering applications, including microscopy, astronomy, and photography. Great work on imaging resolution has been done [1, 2]. From these work, we know that an operating wavelength λ and an aperture D of an imaging system are two key parameters for the resolution [1, 2]. Normally, the resolution is proportional to λ/D , therefore, shorter wavelength and/or larger aperture is required for higher resolution. However, large aperture leads to demanding requirements on the manufacture of a traditional monolithic optical telescope. In order to break the limitation of the conventional monolithic lens, deployable segmented imaging [3], membrane imaging [4], diffractive imaging [5, 6], Fourier-transform telescope [7, 8], interferometric synthetic aperture imaging [9, 10], and lensless imaging [11–23] have been proposed. In these imaging methods, lensless imaging is an appropriate scheme for large aperture (up to decametres and even hectometres) imaging systems, especially for X-ray imaging. In the last few years, lensless point-scanning imaging [11], coher-

ent diffractive imaging [12–15], lensless compressive sensing imaging [16–19], and lensless ghost imaging [20–22] have been proposed. From the viewpoint of classical optical coherence theory, conventional imaging methods are based on first-order correlation, where a point-point corresponding between an object and image planes exists in the first-order field correlation, and the resolution can be directly analyzed from a transmission function of the imaging system. However, for imaging based on wavefront random phase modulation [19, 23–30], where the point-to-point correspondence doesn't exist in first-order field correlation anymore, the resolution is difficult to be directly obtained from the transmission function. Fortunately, when the statistical properties of light fields are known, the resolution may be get by analyzing the high-order correlation of light fields in the viewpoint of ghost imaging (GI, also called as correlated imaging).

The attempt to extract spatial information of an object from high-order correlation of light fields can be traced back to the famous HBT experiment in 1956 [31, 32], which is based on the second-order autocorrelation of light fields in time domain. In

1995, GI [33–37], which is based on the second-order mutual-correlation of light fields between the reference and the test arms, was first demonstrated. It can recover the point-to-point corresponding between the object and image planes from high-order correlation of light fields. The first demonstration of GI with true thermal light was realized by detecting the temporal fluctuations of light fields, and the image of the object is obtained by the second-order mutual-correlation of light fields in time domain [38, 39]. In this scheme, it is required that the temporal resolution of the detector is close to or less than the coherence time of the light field [21, 32], which limits its application in practice. In another scheme for GI with true thermal light, the true thermal light such as sunlight is modulated into a spatially fluctuating pseudo-thermal light field through a spatial random phase modulator, and the image is obtained from the second-order spatial mutual-correlation of light fields [26]. Once the imaging system is calibrated, a 3D data-cube of a spectral image (2D spatial information plus 1D spectral information) can be obtained with a 2D array detector in a single shot with the detection time order-of-magnitude longer than the coherence time [26].

In this paper, based on high-order spatial autocorrelation of thermal light, we propose a lensless Wiener-Khinchin telescope. It can acquire the image of the object in a single shot simply with a spatial random phase modulator. We theoretically and experimentally demonstrate that the resolution not only depends on the aperture of the spatial random phase modulator, but also its statistical properties. The influence of wavelength bandwidth is also investigated. Moreover, imaging for both far and equivalent infinite far away is demonstrated in experiment, which proves the feasibility of lensless Wiener-Khinchin telescope in astronomical observations.

2. METHOD

A. System Schematic

The schematic of a lensless Wiener-Khinchin telescope (Fig. 1) consists of a spatial random phase modulator and a charge-coupled device (CCD) detector, which detects the intensity distribution of the modulated light field. The object is illuminated by a thermal light source.

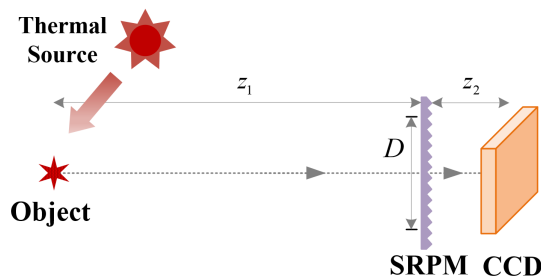


Fig. 1. Schematic of a lensless Wiener-Khinchin telescope. SRPM is an abbreviation of spatial random phase modulator, D is the diameter of the SRPM. z_1 and z_2 are distances from the object and detection planes to the SRPM, respectively.

For incoherent imaging [40], the intensity distribution detected by the CCD detector is

$$I_t(r) = \int_{-\infty}^{\infty} I_0(r_0)h_I(r;r_0)dr_0 \quad (1)$$

where $I_0(r)$ is the intensity distribution in the object plane, $h_I(r;r_0)$ is the incoherent intensity impulse response function, r and r_0 are the coordinates in the detection and the object planes, respectively. Since the target of a telescope is very small compared with the imaging distance, the space translation invariance of system in space (also known as memory effect [41, 42]) is satisfied, so

$$I_t(r) = \int_{-\infty}^{\infty} I_0(r_0)h_I(r;r_0)dr_0 = \{I_0(r_0) \otimes h_I(r_0)\}_{-\frac{z_1}{z_2}r} \quad (2)$$

where \otimes denotes the operation of convolution.

Considering the spatial random phase modulator for thermal light as an ergodic process, the second-order spatial autocorrelation of the measured light field is

$$G_{I_t}^{(2)}(r + \Delta r, r) = \langle E_t^*(r + \Delta r) E_t^*(r) E_t(r) E_t(r + \Delta r) \rangle_r \quad (3) \\ = \overline{\{E_t^*(r + \Delta r) E_t^*(r) E_t(r) E_t(r + \Delta r)\}_s}$$

where $\langle \cdot \rangle_r$ is the spatial average over the coordinate r , and $\overline{\{ \cdot \}_s}$ is the ensemble average of the spatial random phase modulator. Taking Eq. (2) into Eq. (3), we have

$$G_{I_t}^{(2)}(r + \Delta r, r) \\ = \iint_{-\infty}^{\infty} G_h^{(2)}(r + \Delta r, r_0 + \Delta r_0; r, r_0) I_0(r_0 + \Delta r_0) I_0(r_0) dr_0 d\Delta r_0 \quad (4)$$

where

$$G_h^{(2)}(r + \Delta r, r_0 + \Delta r_0; r, r_0) \\ = \overline{\{h_E^*(r + \Delta r; r_0 + \Delta r_0) h_E^*(r; r_0) h_E(r; r_0) h_E(r + \Delta r; r_0 + \Delta r_0)\}_s} \quad (5)$$

is the second-order correlation function of light fields between $h_E(r; r_0)$ and $h_E(r + \Delta r; r_0 + \Delta r_0)$, where the light field $h_E(r; r_0)$ is the point-spread function (PSF).

According to the Central Limit Theorem [43], the light field $h_E(r; r_0)$ through the spatial random phase modulator obeys the complex circular Gaussian distribution in spatial domain [43], and $G_h^{(2)}(r + \Delta r, r_0 + \Delta r_0; r, r_0)$ can be written as [44]

$$G_h^{(2)}(r + \Delta r, r_0 + \Delta r_0; r, r_0) = B \left[1 + g_h^{(2)}(r + \Delta r, r_0 + \Delta r_0; r, r_0) \right] \quad (6)$$

with $B = \overline{\{h_I(r; r_0)\}_s} \overline{\{h_I(r + \Delta r; r_0 + \Delta r_0)\}_s}$, and

$$g_h^{(2)}(r + \Delta r, r_0 + \Delta r_0; r, r_0) = \frac{\overline{\{h_E^*(r + \Delta r; r_0 + \Delta r_0) h_E(r; r_0)\}_s}^2}{B} \quad (7)$$

is defined as the normalized second-order correlation of PSFs.

According to Fresnel diffraction, the PSF of a lensless Wiener-Khinchin telescope is

$$h_E(r; r_0) = \frac{\exp\{j2\pi(z_1 + z_2)/\lambda\}}{-\lambda^2 z_1 z_2} \exp\left\{\frac{j\pi(r - r_0)^2}{\lambda(z_1 + z_2)}\right\} \\ \int_{-\infty}^{\infty} P(r_m) t(r_m) \exp\left\{\frac{j\pi(z_1 + z_2)}{\lambda z_1 z_2} \left[r_m - \frac{z_1 r + z_2 r_0}{z_1 + z_2}\right]^2\right\} dr_m \quad (8)$$

where $P(r_m)$ and $t(r_m) = \exp[j2\pi(n-1)\eta(r_m)/\lambda]$ are the pupil function and the transmission function of the spatial random phase modulator, respectively, while $\eta(r_m)$ and n are the height and the refractive index of the spatial random phase modulator, respectively.

Substituting Eq. (8) into Eq. (7) yields

$$g_h^{(2)}(r + \Delta r, r_0 + \Delta r_0; r, r_0) = \frac{1}{B} \left| \iint_{-\infty}^{\infty} P(r_m) P^*(r_n) \overline{\{t(r_m) t^*(r_n)\}}_s \right. \\ \exp \left\{ j \frac{\pi(z_1 + z_2)}{\lambda z_1 z_2} \left(r_m - \frac{z_1 r + z_2 r_0}{z_1 + z_2} \right)^2 \right\} \\ \left. \exp \left\{ -j \frac{\pi(z_1 + z_2)}{\lambda z_1 z_2} \left(r_n - \frac{z_1(r + \Delta r) + z_2(r_0 + \Delta r_0)}{z_1 + z_2} \right)^2 \right\} dr_m dr_n \right|^2 \quad (9)$$

In general, the height ensemble average $R_\eta(r_m, r_n)$ of the spatial random phase modulator obeys the following mathematical form [45, 46]

$$R_\eta(r_m, r_n) = \overline{\{\eta(r_m) \eta(r_n)\}}_s \\ = \omega^2 \exp \left\{ - \left(\frac{r_m - r_n}{\zeta} \right)^2 \right\} = R_\eta(\Delta r_m), \quad \Delta r_m = r_m - r_n, \quad (10)$$

where ω and ζ are the height standard deviation and the transverse correlation length of the spatial random phase modulator, respectively. Thus, we obtain (see Supplement 1 for details)

$$g_h^{(2)}(r + \Delta r, r_0 + \Delta r_0; r, r_0) \\ \approx \left| \left\{ \exp \left\{ -2 \left[\frac{2\pi(n-1)}{\lambda} \right]^2 \left[\omega^2 - R_\eta \left(\frac{2\lambda z_1 z_2}{z_1 + z_2} \nu \right) \right] \right\} \right. \right. \\ \left. \left. \otimes \mathcal{F} \left\{ |P(\mu + \mu_0)|^2 \right\}_{\mu \rightarrow \nu} \right\} \frac{z_1 \Delta r + z_2 \Delta r_0}{2\lambda z_1 z_2} \right|^2 \\ = g_h^{(2)} \left(\frac{z_1 \Delta r + z_2 \Delta r_0}{2\lambda z_1 z_2} \right), \quad (11)$$

where $\mathcal{F}\{\dots\}_{\mu \rightarrow \nu}$ represents the Fourier transform of the function with the variable μ and the transformed function variable is ν , and

$$\mu_0 = \frac{z_1(2r + \Delta r) + z_2(2r_0 + \Delta r_0)}{2(z_1 + z_2)}. \quad (12)$$

Taking Eqs. (6) and (11) into Eq. (4), we have

$$G_{I_t}^{(2)}(r + \Delta r, r) \\ \approx B \left\{ \left[1 + g_h^{(2)} \left(\frac{\Delta r_0}{2\lambda z_1} \right) \right] \otimes G_{I_0}^{(2)}(r_0 + \Delta r_0, r_0) \right\} \frac{z_1}{z_2} \Delta r, \quad (13)$$

where

$$G_{I_0}^{(2)}(r_0 + \Delta r_0, r_0) = \langle I_0(r_0 + \Delta r_0) I_0(r_0) \rangle_{r_0} \\ = \int_{-\infty}^{\infty} I_0(r_0) I_0(r_0 + \Delta r_0) dr_0, \quad (14)$$

and

$$g_h^{(2)} \left(\frac{\Delta r_0}{2\lambda z_1} \right) \\ = \left| \left\{ \exp \left\{ -2 \left[\frac{2\pi(n-1)}{\lambda} \right]^2 \left[\omega^2 - R_\eta \left(\frac{2\lambda z_1 z_2}{z_1 + z_2} \nu \right) \right] \right\} \right. \right. \\ \left. \left. \otimes \mathcal{F} \left\{ |P(\mu + \mu_0)|^2 \right\}_{\mu \rightarrow \nu} \right\} \frac{\Delta r_0}{2\lambda z_1} \right|^2. \quad (15)$$

Since the thermal light source can be considered as an ergodic random process, the spatial autocorrelation function of $I_0(r_0)$ is equal to the statistical autocorrelation function. According to the Wiener-Khinchin theorem [47, 48], we have

$$G_{I_0}^{(2)}(r_0 + \Delta r_0, r_0) = \mathcal{F}^{-1} \left\{ \left\{ \overline{\left| \mathcal{F} \{ I_0(r_0) \}_{r_0 \rightarrow f_0} \right|^2} \right\}_t \right\}_{f_0 \rightarrow \Delta r_0}, \quad (16)$$

where $\overline{\{\cdot\}}_t$ denotes the statistical autocorrelation of thermal light. Substituting Eq. (16) into Eq. (13), we obtain

$$G_{I_t}^{(2)}(r + \Delta r, r) \propto \left\{ \left[1 + g_h^{(2)} \left(\frac{\Delta r_0}{2\lambda z_1} \right) \right] \right. \\ \left. \otimes \mathcal{F}^{-1} \left\{ \left\{ \overline{\left| \mathcal{F} \{ I_0(r_0) \}_{r_0 \rightarrow f_0} \right|^2} \right\}_t \right\}_{f_0 \rightarrow \Delta r_0} \right\} \frac{z_1}{z_2} \Delta r. \quad (17)$$

Eq. (17) indicates that the power spectral density $\left\{ \overline{\left| \mathcal{F} \{ I_0(r_0) \}_{r_0 \rightarrow f_0} \right|^2} \right\}_t$ of the intensity distribution $I_0(r_0)$ on the object plane can be separated from $G_{I_t}^{(2)}(r + \Delta r, r)$, and the resolution is determined by $g_h^{(2)} \left(\frac{\Delta r_0}{2\lambda z_1} \right)$. The image of $I_0(r_0)$ can be reconstructed by utilizing phase retrieval algorithms [49–58]. Here, only amplitude information of an object is interested, which can be used as a constraint to greatly improve the speed and quality of reconstruction [59].

3. SYSTEM ANALYSIS

To quantify the imaging system, the relationship between the field of view (FOV), the resolution and the spatial random phase modulator is analyzed.

A. Field of View

The FOV of lensless Wiener-Khinchin telescope is limited by the memory effect range of the imaging system [41, 42, 60, 61]. Considering the height standard deviation ω of the spatial random phase modulator, the normalized second-order correlation function of light fields between different incident angles without transverse translation is given by (see Supplement 1 for details)

$$g_\theta^{(2)}(\Delta\theta) = \exp \left\{ - \left[\frac{2\pi\omega}{\lambda} \left(\sqrt{n^2 - \sin^2(\Delta\theta)} - n \right) \right]^2 \right\} \\ \approx \exp \left\{ - \left(\frac{\pi n \omega}{\lambda} \sin^2(\Delta\theta) \right)^2 \right\}, \quad (18)$$

where $\Delta\theta$ is the variation of the incident angle. According to Eq. (18), the FOV of lensless Wiener-Khinchin telescope is proportional to $\frac{\lambda}{\omega}$.

In addition, Eq. (17) leads to a limitation of the FOV of lensless Wiener-Khinchin telescope,

$$FOV < \frac{L}{z_2} \quad (19)$$

with L denoting the CCD detector size. This equation indicates that FOV is also limited by the CCD detector size. In order to obtain a large FOV, the CCD detector size of lensless Wiener-Khinchin telescope is required to be much larger than $\frac{\lambda z_2}{\omega}$ in Eq. (18).

B. Resolution

Eq. (15) indicates that the resolution not only depends on the aperture of the spatial random phase modulator, but also its statistical properties. According to the convolution operation in $g_h^{(2)}\left(\frac{\Delta r_0}{2\lambda z_1}\right)$, we discuss two simple cases in the following contents, where the resolution is mainly limited by the aperture and the statistical properties of the spatial random phase modulator, respectively.

B.1. Case 1: resolution is mainly limited by the aperture.

When the full width at half maximum (FWHM) of $\exp\left\{-2\left[\frac{2\pi(n-1)}{\lambda}\right]^2\left[\omega^2 - R_\eta\left(\frac{2\lambda z_1 z_2}{z_1 + z_2}\nu\right)\right]\right\}$ is much smaller than the FWHM of $\mathcal{F}\{|P(\mu + \mu_0)|^2\}_{\mu \rightarrow \nu}$, we have

$$\begin{aligned} g_h^{(2)}\left(\frac{\Delta r_0}{2\lambda z_1}\right) &\approx \left| \mathcal{F}\{|P(\mu + \mu_0)|^2\}_{\mu \rightarrow -\frac{\Delta r_0}{2\lambda z_1}} \right|^2 \\ &= \left| \mathcal{F}\{|P(\mu)|^2\}_{\mu \rightarrow -\frac{\Delta r_0}{2\lambda z_1}} \right|^2. \end{aligned} \quad (20)$$

For a circle aperture of the spatial random phase modulator, $P(\mu) = \text{circ}\left(\frac{\mu}{D}\right)$, and this leads to

$$g_h^{(2)}\left(\frac{\Delta r_0}{2\lambda z_1}\right) \propto \left[\frac{J_1\left(\frac{2\pi D \Delta r_0}{z_1 \lambda}\right)}{\frac{2\pi D \Delta r_0}{z_1 \lambda}} \right]^2. \quad (21)$$

Under this condition, the resolution of the lensless Wiener-Khinchin telescope is proportional to $\lambda z_1/D$.

B.2. Case 2: resolution is mainly limited by the statistical properties.

When the FWHM of $\exp\left\{-2\left[\frac{2\pi(n-1)}{\lambda}\right]^2\left[\omega^2 - R_\eta\left(\frac{2\lambda z_1 z_2}{z_1 + z_2}\nu\right)\right]\right\}$ is much larger than the FWHM of $\mathcal{F}\{|P(\mu + \mu_0)|^2\}_{\mu \rightarrow \nu}$,

$$\begin{aligned} &g_h^{(2)}\left(\frac{\Delta r_0}{2\lambda z_1}\right) \\ &\approx \exp\left\{-4\left[\frac{2\pi(n-1)\omega}{\lambda}\right]^2\left\{1 - \exp\left\{-\left[\frac{z_2 \Delta r_0}{(z_1 + z_2)\zeta}\right]^2\right\}\right\}\right\} \\ &\approx \exp\left\{-4\left[\frac{2\pi(n-1)\omega z_2 \Delta r_0}{\lambda(z_1 + z_2)\zeta}\right]^2\right\}, \end{aligned} \quad (22)$$

where the first-order approximation $\exp\left\{-\left[\frac{z_2 \Delta r_0}{(z_1 + z_2)\zeta}\right]^2\right\} \approx 1 - \left[\frac{z_2 \Delta r_0}{(z_1 + z_2)\zeta}\right]^2$. Under this condition, the resolution is proportional to $\left(1 + \frac{z_1}{z_2}\right) \frac{\lambda \zeta}{(n-1)\omega}$.

For digital images, the reconstruction is also affected by the pixel size of the CCD detector. Due to Eq. (17), the pixel size P_{CCD} of the CCD detector is required by

$$P_{CCD} < \frac{z_2}{M z_1} g_h^{(2)}\left(\frac{\Delta r_0}{2\lambda z_1}\right), \quad (23)$$

where M denotes a split number for discrimination of resolution. For *Case 1*, according to Eq. (21), the FWHM of $g_h^{(2)}\left(\frac{\Delta r_0}{2\lambda z_1}\right)$ is proportional to $\lambda z_1/D$, and taking this result into Eq. (23), the pixel size of CCD detector is required to be smaller than $\frac{\lambda z_2}{MD}$. Similarly, for *Case 2*, the pixel size of CCD detector is required to be smaller than $\frac{\lambda \zeta}{M(n-1)\omega}$ with $z_1 \gg z_2$ in a telescope scheme.

4. EXPERIMENTAL VALIDATION

The experimental setup is shown in Fig. 2. An object is illuminated by a xenon lamp. The reflected light is filtered by a narrow-band filter, and modulated by a spatial random phase modulator with a height standard deviation $\omega = 1 \mu\text{m}$, a transverse correlation length $\zeta = 44 \mu\text{m}$ and the refractive index $n = 1.46$, and then relayed by a lens with a magnification factor $\beta = 10$ and a numerical aperture $N.A. = 0.25$ onto a CCD detector (APGCCD) with a pixel size $13 \mu\text{m} \times 13 \mu\text{m}$, which records the magnified intensity distribution. The lens is only used to amplify the intensity distribution to match the pixel size of the CCD detector, and is not necessary in some conditions.

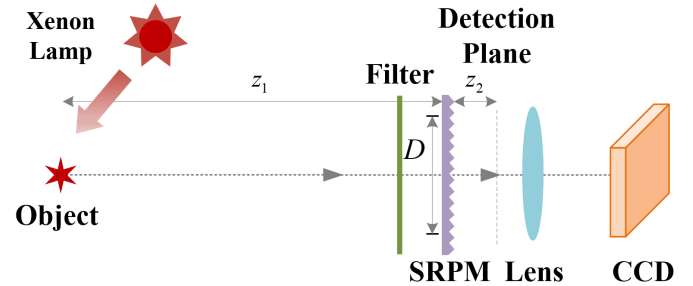


Fig. 2. Experimental setup of lensless Wiener-Khinchin telescope.

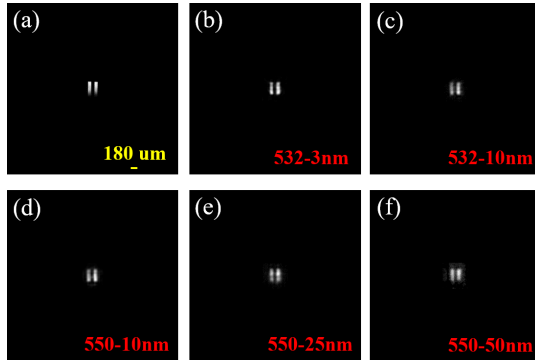


Fig. 3. Experimental results with different narrow-band filters. (a) A photograph of the double slit, where a yellow scale bar is inserted in the low right corner. Reconstructed images with different narrow-band filters: (b) $\lambda = 532$ nm, $w = 3$ nm, (c) $\lambda = 532$ nm, $w = 10$ nm, (d) $\lambda = 550$ nm, $w = 10$ nm, (e) $\lambda = 550$ nm, $w = 25$ nm, (f) $\lambda = 550$ nm, $w = 50$ nm.

In order to analyze the resolution of the system, a double slit (shown in Fig. 3(a)) is selected. Since the image is obtained from the second-order spatial autocorrelation of thermal light, the temporal coherence is not strictly required. But the temporal coherence of the light field still affects the contrast of the spatial fluctuating pseudo-thermal light due to the dispersion of the spatial random phase modulator. The reflected light from the object is filtered by a narrow-band filter, whose central wavelength λ is either 532 nm or 550 nm, and its bandwidth w varies among 3 nm, 10 nm, 25 nm and 50 nm, when $z_1 = 0.15$ m, $z_2 = 12$ mm, and $D = 8$ mm. The results with the same phase retrieval algorithm [52] are shown in Fig. 3. The experimental results show that the situation is better for narrow band light. In subsequent experiments, a narrow-band filter with a center wavelength $\lambda = 532$ nm and a bandwidth $w = 10$ nm is selected.

To verify Eq. (21) in experiment, the aperture size is changed. Images with five different apertures $D = 4$ mm, 4.5 mm, 5 mm, 6 mm, 8 mm are obtained, respectively, while $z_1 = 1.1$ m and $z_2 = 60$ mm are selected in accordance with *Case 1* (see Fig. 4(a)-(e)). According to Eq. (21), the theoretical resolutions with different apertures are shown in Fig. 4(f), where FWHMs for $D = 4$ mm, 4.5 mm, 5 mm, 6 mm and 8 mm are 150 μ m, 134 μ m, 121 μ m, 100 μ m and 75 μ m, respectively. Fig. 4(g) shows a comparison of theoretical and experimental resolutions at $D = 5$ mm, where the red line is a cross-section denoted by the dash line in Fig. 4(c). The experimental results show that the double slit can be distinguished at $D = 5$ mm, which agrees well with theoretical results.

In *Case 2*, the resolution is mainly affected by the statistical properties of the spatial random phase modulator, which leads to a limitation of z_2 based on Eq. (22). Five different z_2 (4 mm, 6 mm, 8 mm, 10 mm, 12 mm) are selected, and the reconstructed images are shown in Fig. 5(a)-(e), while $z_1 = 0.3$ m and $D = 8$ mm. The corresponding theoretical resolutions are shown in Fig. 5(f), where FWHMs for $z_2 = 4$ mm, 6 mm, 8 mm, 10 mm and 12 mm are 313 μ m, 211 μ m, 160 μ m, 129 μ m and 108 μ m, respectively. Fig. 5(g) shows a comparison of theoretical and experimental resolutions at $z_2 = 8$ mm, where the red line is the cross-section denoted by the dash line in Fig. 5(c). The results show that the double slit can be distinguished at $z_2 = 8$ mm.

To further verify the imaging capability of lensless Wiener-

Khinchin telescope, two targets, a letter π and a panda toy, are imaged, respectively. Different system parameters are selected for the two targets at $D = 8$ mm. For the ' π ', $z_1 = 0.5$ m, $z_2 = 2$ mm, and for the 'panda', $z_1 = 1.5$ m, $z_2 = 3$ mm. The reconstructed images of both are shown in Fig. 6.

For astronomical observations, the distance z_1 is nearly infinitely far away, which means $z_1 \gg z_2$, so the resolution $g_h^{(2)}\left(\frac{\Delta r_0}{2\lambda z_1}\right)$ in Eq. (15) is approximated to

$$g_h^{(2)}\left(\frac{\Delta r_0}{2\lambda z_1}\right) \propto \left\{ \exp\left\{-2\left[\frac{2\pi(n-1)}{\lambda}\right]^2\left[\omega^2 - R_\eta(2\lambda z_2 \nu)\right]\right\} \otimes \mathcal{F}\left\{|P(\mu)|^2\right\}_{\mu \rightarrow \nu}\right\}_{\frac{\Delta r_0}{2\lambda z_1}}^2. \quad (24)$$

An object 'GI' is placed on the focal plane of an optical lens before the spatial random phase modulator to experimentally simulate the target placed infinite far away. The image can be well reconstructed, as shown in Fig. 7. Imaging for both far and equivalent infinite far away demonstrated in Figs. 6 and 7 proves the feasibility of lensless Wiener-Khinchin telescope in astronomical observations.

5. CONCLUSION

In this paper, we propose and demonstrate a novel optical imaging system, the lensless Wiener-Khinchin telescope based on high-order spatial autocorrelation of thermal light. We analyze the high-order correlation function, and obtain a quantitative description of the resolution and FOV, which will provide a system design guide for practice applications. Compared with lensless compressive sensing imaging [16-19] and lensless GI [20-22], neither a measurement matrix nor a calibration process is required. Thus the lensless Wiener-Khinchin telescope has conspicuous advantages in applications such as astronomical observations, where the calibration for an unknown imaging distance is difficult and inaccurate. The cancellation of calibration also results in lower requirements in system stability. Meanwhile, a tabletop lensless Wiener-Khinchin telescope for X-ray is also approachable with developments of material technology, which make more materials such as abrasive paper can be used as a spatial random phase modulator for X-ray [62, 63]. Moreover, considering the scattering medium as a spatial random phase modulator, lensless Wiener-Khinchin telescope may also open a door to quantitatively describe imaging through scattering medium [23, 64-67].

FUNDING

National Key Research and Development Program of China (2017YFB0503303). Hi-Tech Research and Development Program of China (2013AA122902 and 2013AA122901).

ACKNOWLEDGMENTS

We thank Guowei Li and Guohai Situ for helpful discussions.

See [Supplement 1](#) for supporting content.

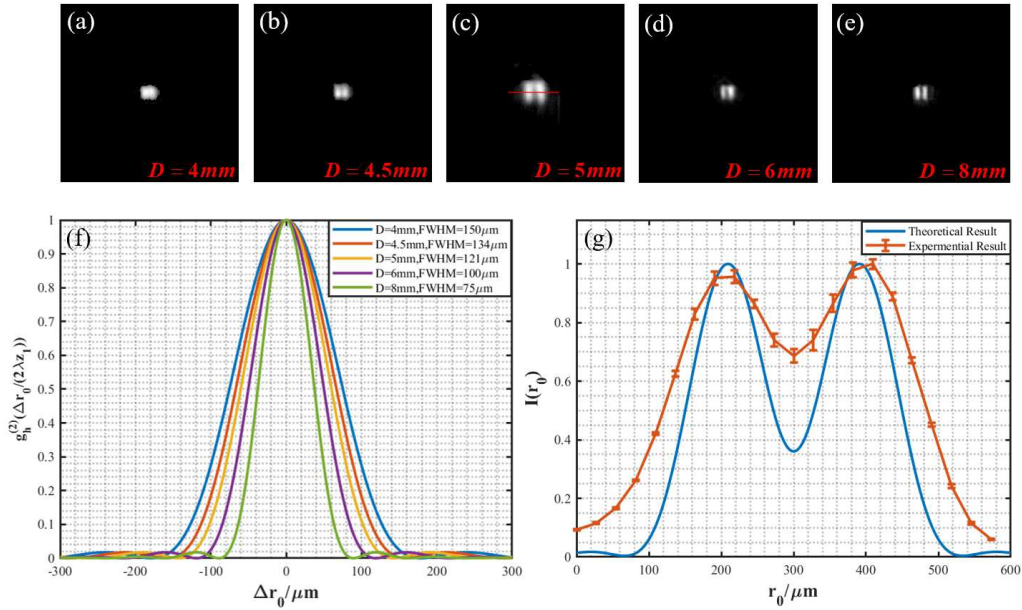


Fig. 4. Resolution at different apertures of the spatial random phase modulator. Reconstructed images with different apertures: (a) $D = 4\text{ mm}$, (b) $D = 4.5\text{ mm}$, (c) $D = 5\text{ mm}$, (d) $D = 6\text{ mm}$, (e) $D = 8\text{ mm}$. (f) The theoretical resolutions. (g) A comparison between theoretical and experimental resolutions at $D = 5\text{ mm}$, and the red line is a cross-section denoted by the dash line in Fig. 4(c).

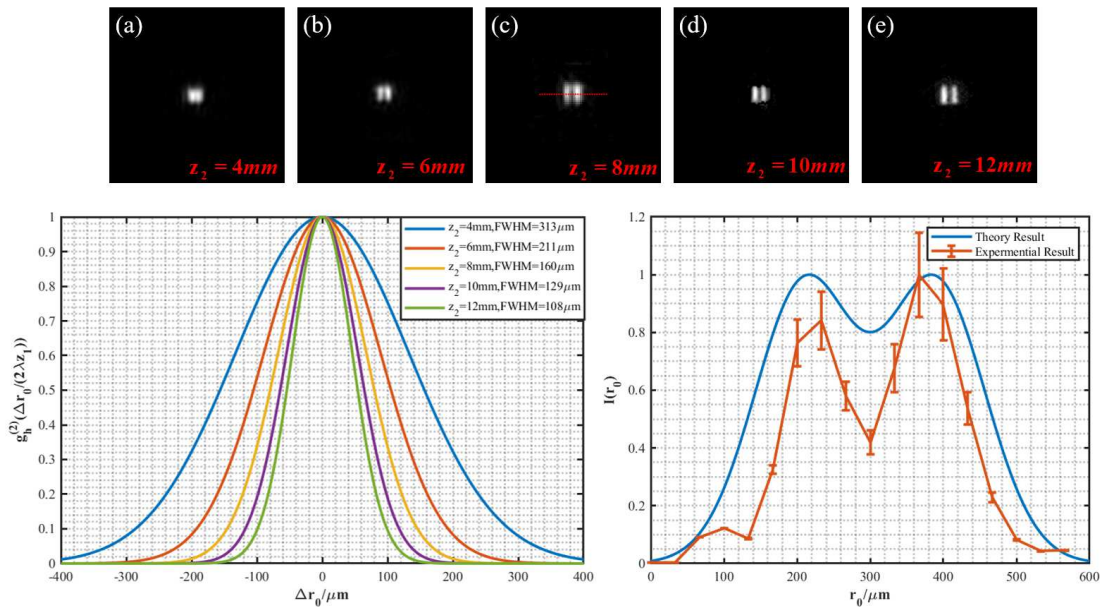


Fig. 5. Resolution at different z_2 . Reconstructed images with different z_2 : (a) $z_2 = 4\text{ mm}$, (b) $z_2 = 6\text{ mm}$, (c) $z_2 = 8\text{ mm}$, (d) $z_2 = 10\text{ mm}$, (e) $z_2 = 12\text{ mm}$. (f) The theoretical resolutions. (g) A comparison between theoretical and experimental resolutions at $z_2 = 8\text{ mm}$, and the red line is a cross-section denoted by the dash line in Fig. 5(c).

REFERENCES

1. C. J. R. Sheppard, "Resolution and super-resolution," *Microsc. Res. Tech.* **80**, 590–598 (2017).
2. S. Baker and T. Kanade, "Limits on super-resolution and how to break them," *IEEE Transactions on Pattern Analysis Mach. Intell.* **24**, 1167–1183 (2002).
3. M. A. Greenhouse, "The JWST science instrument payload: mission context and status," in "UV/Optical/IR Space Telescopes and Instruments: Innovative Technologies and Concepts VII," H. A. MacEwen and J. B. Breckinridge, eds. (SPIE, 2015).
4. M. Angel, "Eight-inch f5 deformable magnetic-membrane mirror," in "Optomechanical Technologies for Astronomy," E. Atad-Ettinger, J. Antebi, and D. Lemke, eds. (SPIE, 2006).
5. R. A. Hyde, "Eyeglass 1 very large aperture diffractive telescopes," *Appl. Opt.* **38**, 4198 (1999).
6. P. D. Atcheson, C. Stewart, J. Domber, K. Whiteaker, J. Cole, P. Spuhler, A. Seltzer, J. A. Britten, S. N. Dixit, B. Farmer, and L. Smith, "MOIRE: initial demonstration

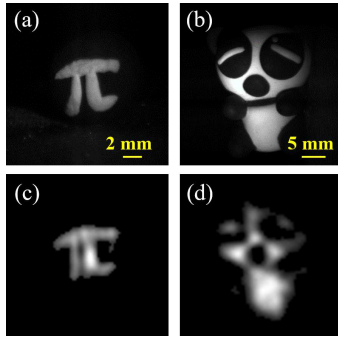


Fig. 6. Imaging a letter π and a panda toy. (a) and (b) are photographs, where a yellow scale bar is inserted in the low right corner, respectively. (c) and (d) are reconstructed images, respectively.

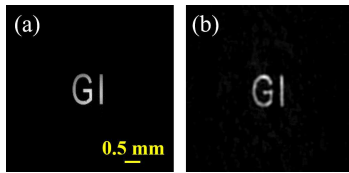


Fig. 7. Imaging an object placed equivalent infinite far away. (a) A photograph of the target, where a yellow scale bar is inserted in the low right corner, (b) reconstructed image.

of a transmissive diffractive membrane optic for large lightweight optical telescopes," in "Space Telescopes and Instrumentation 2012: Optical, Infrared, and Millimeter Wave," M. C. Clampin, G. G. Fazio, H. A. MacEwen, and J. M. Oschmann, eds. (SPIE, 2012).

7. T. A. Prince, G. J. Hurford, H. S. Hudson, and C. J. Crannell, "Gamma-ray and hard x-ray imaging of solar flares," *Sol. Phys.* **118**, 269–290 (1988).
8. T. Kosugi, K. Makishima, T. Murakami, T. Sakao, T. Dotani, M. Inada, K. Kai, S. Masuda, H. Nakajima, Y. Ogawara, M. Sawa, and K. Shibasaki, "The hard x-ray telescope (HXT) for the SOLAR-a mission," in "The Yohkoh (Solar-A) Mission," (Springer Netherlands, 1991), pp. 17–36.
9. A. B. Meinel, "Aperture synthesis using independent telescopes," *Appl. Opt.* **9**, 2501 (1970).
10. C. Fridlund, "Darwin-the infrared space interferometry mission," *Eur. Space Agency Special Publ. SP* (2000).
11. Y. Cui, S. Schuon, D. Chan, S. Thrun, and C. Theobalt, "3d shape scanning with a time-of-flight camera," in "2010 IEEE Computer Society Conference on Computer Vision and Pattern Recognition," (IEEE, 2010).
12. J. Miao, P. Charalambous, J. Kirz, and D. Sayre, "Extending the methodology of x-ray crystallography to allow imaging of micrometre-sized non-crystalline specimens," *Nature* **400**, 342–344 (1999).
13. H. N. Chapman and K. A. Nugent, "Coherent lensless x-ray imaging," *Nat. Photonics* **4**, 833–839 (2010).
14. B. Abbey, L. W. Whitehead, H. M. Quiney, D. J. Vine, G. A. Cadenazzi, C. A. Henderson, K. A. Nugent, E. Balaur, C. T. Putkunz, A. G. Peele, G. J. Williams, and I. McNulty, "Lensless imaging using broadband x-ray sources," *Nat. Photonics* **5**, 420–424 (2011).
15. J. Miao, T. Ishikawa, I. K. Robinson, and M. M. Murnane, "Beyond crystallography: Diffractive imaging using coherent

x-ray light sources," *Science* **348**, 530–535 (2015).

16. A. Zomet and S. Nayar, "Lensless imaging with a controllable aperture," in "2006 IEEE Computer Society Conference on Computer Vision and Pattern Recognition - Volume 1 (CVPR'06)," (IEEE, 2006).
17. G. Huang, H. Jiang, K. Matthews, and P. Wilford, "Lensless imaging by compressive sensing," in "2013 IEEE International Conference on Image Processing," (IEEE, 2013).
18. M. S. Asif, A. Ayremlou, A. Sankaranarayanan, A. Veeraraghavan, and R. G. Baraniuk, "FlatCam: Thin, lensless cameras using coded aperture and computation," *IEEE Transactions on Comput. Imaging* **3**, 384–397 (2017).
19. N. Antipa, G. Kuo, R. Heckel, B. Mildenhall, E. Bostan, R. Ng, and L. Waller, "DiffuserCam: lensless single-exposure 3d imaging," *Optica* **5**, 1 (2017).
20. X. H. Chen, Q. Liu, K. H. Luo, and L. A. Wu, "Lensless ghost imaging with true thermal light," *Opt. Lett.* **34**, 695 (2009).
21. X. F. Liu, X. H. Chen, X. R. Yao, W. K. Yu, G. J. Zhai, and L. A. Wu, "Lensless ghost imaging with sunlight," *Opt. Lett.* **39**, 2314 (2014).
22. H. Yu, R. Lu, S. Han, H. Xie, G. Du, T. Xiao, and D. Zhu, "Fourier-transform ghost imaging with hard x rays," *Phys. Rev. Lett.* **117** (2016).
23. O. Katz, P. Heidmann, M. Fink, and S. Gigan, "Non-invasive single-shot imaging through scattering layers and around corners via speckle correlations," *Nat. Photonics* **8**, 784–790 (2014).
24. A. Liutkus, D. Martina, S. Popoff, G. Chardon, O. Katz, G. Lerosey, S. Gigan, L. Daudet, and I. Carron, "Imaging with nature: compressive imaging using a multiply scattering medium," *Sci. Reports* **4** (2014).
25. H. Yilmaz, E. G. van Putten, J. Bertolotti, A. Lagendijk, W. L. Vos, and A. P. Mosk, "Speckle correlation resolution enhancement of wide-field fluorescence imaging," *Optica* **2**, 424 (2015).
26. Z. Liu, S. Tan, J. Wu, E. Li, X. Shen, and S. Han, "Spectral camera based on ghost imaging via sparsity constraints," *Sci. Reports* **6** (2016).
27. S. K. Sahoo, D. Tang, and C. Dang, "Single-shot multi-spectral imaging with a monochromatic camera," *Optica* **4**, 1209 (2017).
28. J. K. Adams, V. Boominathan, B. W. Avants, D. G. Vercosa, F. Ye, R. G. Baraniuk, J. T. Robinson, and A. Veeraraghavan, "Single-frame 3d fluorescence microscopy with ultraminiature lensless FlatScope," *Sci. Adv.* **3**, e1701548 (2017).
29. S. Mukherjee, A. Vijayakumar, M. Kumar, and J. Rosen, "3d imaging through scatterers with interferenceless optical system," *Sci. Reports* **8** (2018).
30. P. Wang and R. Menon, "Ultra-high-sensitivity color imaging via a transparent diffractive-filter array and computational optics," *Optica* **2**, 933 (2015).
31. R. H. Brown and R. Q. Twiss, "Correlation between photons in two coherent beams of light," *Nature* **177**, 27–29 (1956).
32. R. H. Brown and R. Q. Twiss, "The question of correlation between photons in coherent light rays," *Nature* **178**, 1447–1448 (1956).
33. D. V. Strekalov, A. V. Sergienko, D. N. Klyshko, and Y. H. Shih, "Observation of two-photon "ghost" interference and diffraction," *Phys. Rev. Lett.* **74**, 3600–3603 (1995).
34. A. Gatti, E. Brambilla, M. Bache, and L. A. Lugiato, "Ghost imaging with thermal light: comparing entanglement and

- classical correlation," *Phys. Rev. Lett.* **93** (2004).
35. J. Cheng and S. Han, "Incoherent coincidence imaging and its applicability in x-ray diffraction," *Phys. Rev. Lett.* **92** (2004).
 36. J. H. Shapiro, "Computational ghost imaging," *Phys. Rev. A* **78**, 061802 (2008).
 37. J. H. Shapiro and R. W. Boyd, "The physics of ghost imaging," *Quantum Inf. Process.* **11**, 949–993 (2012).
 38. A. Valencia, G. Scarcelli, M. D'Angelo, and Y. Shih, "Two-photon imaging with thermal light," *Phys. Rev. Lett.* **94** (2005).
 39. D. Zhang, Y. H. Zhai, L. A. Wu, and X. H. Chen, "Correlated two-photon imaging with true thermal light," *Opt. Lett.* **30**, 2354 (2005).
 40. J. W. Goodman, *Introduction to Fourier optics*, 154-160 (Roberts and Company Publishers, 2005).
 41. S. Feng, C. Kane, P. A. Lee, and A. D. Stone, "Correlations and fluctuations of coherent wave transmission through disordered media," *Phys. Rev. Lett.* **61**, 834–837 (1988).
 42. G. Osnabrugge, R. Horstmeyer, I. N. Papadopoulos, B. Judkewitz, and I. M. Vellekoop, "Generalized optical memory effect," *Optica*, **4**, 886 (2017).
 43. J. W. Goodman, *Speckle phenomena in optics: theory and applications*, 9-12 (Roberts and Company Publishers, 2007).
 44. J. W. Goodman, *Statistical optics*, 44 (John Wiley & Sons, New York, 2015).
 45. S. K. Sinha, E. B. Sirota, S. Garoff, and H. B. Stanley, "X-ray and neutron scattering from rough surfaces," *Phys. Rev. B* **38**, 2297–2311 (1988).
 46. Y. P. Zhao, I. Wu, C. F. Cheng, U. Block, G. C. Wang, and T. M. Lu, "Characterization of random rough surfaces by in-plane light scattering," *J. Appl. Phys.* **84**, 2571–2582 (1998).
 47. L. Cohen, "The generalization of the wiener-khinchin theorem," in "Proceedings of the 1998 IEEE International Conference on Acoustics, Speech and Signal Processing, ICASSP '98 (Cat. No.98CH36181)," (IEEE, 1998).
 48. J. W. Goodman, *Statistical optics*, 73-79 (John Wiley & Sons, New York, 2015).
 49. J. R. Fienup, "Reconstruction of an object from the modulus of its fourier transform," *Opt. Lett.* **3**, 27 (1978).
 50. J. R. Fienup, "Phase retrieval algorithms: a comparison," *Appl. Opt.* **21**, 2758 (1982).
 51. E. J. Candès, T. Strohmer, and V. Voroninski, "PhaseLift: exact and stable signal recovery from magnitude measurements via convex programming," *Commun. on Pure Appl. Math.* **66**, 1241–1274 (2012).
 52. X. Liu, J. Wu, W. He, M. Liao, C. Zhang, and X. Peng, "Vulnerability to ciphertext-only attack of optical encryption scheme based on double random phase encoding," *Opt. Express* **23**, 18955 (2015).
 53. Y. Chen and E. Candès, "Solving random quadratic systems of equations is nearly as easy as solving linear systems," in "Advances in Neural Information Processing Systems 28," C. Cortes, N. D. Lawrence, D. D. Lee, M. Sugiyama, and R. Garnett, eds. (Curran Associates, Inc., 2015), pp. 739–747.
 54. Y. Shechtman, Y. C. Eldar, O. Cohen, H. N. Chapman, J. Miao, and M. Segev, "Phase retrieval with application to optical imaging: a contemporary overview," *IEEE Signal Process. Mag.* **32**, 87–109 (2015).
 55. E. J. Candès, Y. C. Eldar, T. Strohmer, and V. Voroninski, "Phase retrieval via matrix completion," *SIAM Rev.* **57**, 225–251 (2015).
 56. E. J. Candès, X. Li, and M. Soltanolkotabi, "Phase retrieval via wirtinger flow: theory and algorithms," *IEEE Transactions on Inf. Theory* **61**, 1985–2007 (2015).
 57. E. J. Candès, X. Li, and M. Soltanolkotabi, "Phase retrieval from coded diffraction patterns," *Appl. Comput. Harmon. Analysis* **39**, 277–299 (2015).
 58. K. Jaganathan, S. Oymak, and B. Hassibi, "Sparse phase retrieval: uniqueness guarantees and recovery algorithms," *IEEE Transactions on Signal Process.* **65**, 2402–2410 (2017).
 59. G. Ying, Q. Wei, X. Shen, and S. Han, "A two-step phase-retrieval method in fourier-transform ghost imaging," *Opt. Commun.* **281**, 5130–5132 (2008).
 60. D. Léger, E. Mathieu, and J. C. Perrin, "Optical surface roughness determination using speckle correlation technique," *Appl. Opt.* **14**, 872 (1975).
 61. B. Judkewitz, R. Horstmeyer, I. M. Vellekoop, I. N. Papadopoulos, and C. Yang, "Translation correlations in anisotropically scattering media," *Nat. Phys.* **11**, 684–689 (2015).
 62. M.-C. Zdora, P. Thibault, F. Pfeiffer, and I. Zanette, "Simulations of x-ray speckle-based dark-field and phase-contrast imaging with a polychromatic beam," *J. Appl. Phys.* **118**, 113105 (2015).
 63. A. X. Zhang, Y. H. He, L. A. Wu, L. M. Chen, and B. B. Wang, "Tabletop x-ray ghost imaging with ultra-low radiation," *Optica*, **5**, 374 (2018).
 64. J. Bertolotti, E. G. van Putten, C. Blum, A. Lagendijk, W. L. Vos, and A. P. Mosk, "Non-invasive imaging through opaque scattering layers," *Nature*, **491**, 232–234 (2012).
 65. O. Katz, E. Small, and Y. Silberberg, "Looking around corners and through thin turbid layers in real time with scattered incoherent light," *Nat. Photonics* **6**, 549–553 (2012).
 66. X. Yang, Y. Pu, and D. Psaltis, "Imaging blood cells through scattering biological tissue using speckle scanning microscopy," *Opt. Express* **22**, 3405 (2014).
 67. H. Zhuang, H. He, X. Xie, and J. Zhou, "High speed color imaging through scattering media with a large field of view," *Sci. Reports* **6** (2016).